NEOPLASIA
www.neoplasia.com

Volume 19 Number 5 May 2017 pp. 439–450 439

# DDK Promotes Tumor Chemoresistance and Survival via Multiple Pathways

**Nanda Kumar Sasi[*,†,‡], Arjun Bhutkar[§], Nathan J. Lanning[†], Jeffrey P. MacKeigan[†] and Michael Weinreich[*]**

*Laboratory of Genome Integrity and Tumorigenesis, Van Andel Research Institute (VARI), Grand Rapids, MI 49503; [†]Laboratory of Systems Biology, VARI; [‡]Graduate Program in Genetics, Michigan State University, East Lansing, MI 48824; [§]David H. Koch Institute for Integrative Cancer Research, Department of Biology, Massachusetts Institute of Technology, Cambridge, MA 02139, USA

## Abstract

DBF4-dependent kinase (DDK) is a two-subunit kinase required for initiating DNA replication at individual origins and is composed of CDC7 kinase and its regulatory subunit DBF4. Both subunits are highly expressed in many diverse tumor cell lines and primary tumors, and this is correlated with poor prognosis. Inhibiting DDK causes apoptosis of tumor cells, but not normal cells, through a largely unknown mechanism. Firstly, to understand why DDK is often overexpressed in tumors, we identified gene expression signatures that correlate with DDK high- and DDK low-expressing lung adenocarcinomas. We found that increased DDK expression is highly correlated with inactivation of RB1-E2F and p53 tumor suppressor pathways. Both *CDC7* and *DBF4* promoters bind E2F, suggesting that increased E2F activity in *RB1* mutant cancers promotes increased DDK expression. Surprisingly, increased DDK expression levels are also correlated with both increased chemoresistance and genome-wide mutation frequencies. Our data further suggest that high DDK levels directly promote elevated mutation frequencies. Secondly, we performed an RNAi screen to investigate how DDK inhibition causes apoptosis of tumor cells. We identified 23 kinases and phosphatases required for apoptosis when DDK is inhibited. These hits include checkpoint genes, G2/M cell cycle regulators, and known tumor suppressors leading to the hypothesis that inhibiting mitotic progression can protect against DDKi-induced apoptosis. Characterization of one novel hit, the LATS2 tumor suppressor, suggests that it promotes apoptosis independently of the upstream MST1/2 kinases in the Hippo signaling pathway.

*Neoplasia (2017) 19, 439–450*

## Introduction

Increased proliferative capacity and evasion from growth suppressors are classic hallmarks of tumorigenesis [1]. Tumors can evade growth suppression by mutating key gatekeeper proteins that are responsible for activating cell cycle checkpoints. However, unchecked cell cycle progression can result in genome instability arising from errors in DNA replication, DNA repair, or chromosome segregation. This genome instability furthers tumor growth and evolution through increased mutation rates, chromosomal rearrangements, and genome-wide amplification events [1]. Tumor cells evolve several mechanisms to tolerate genomic instability, frequently by increasing the expression and activity of DNA repair proteins or by altering key cell cycle regulatory proteins. In fact, altered DNA repair pathways have been identified as key drivers of tumorigenesis [2].

DBF4-dependent kinase (DDK) is a key cell cycle protein required for DNA replication by catalyzing MCM helicase activation at each individual replication origin during S-phase [3]. DDK is composed of CDC7 kinase and its regulatory subunit DBF4, which is required for

Abbreviations: DDK, DBF4-dependent kinase; LATS2, large tumor suppressor kinase 2; TCGA, The Cancer Genome Atlas

Address all correspondence to: Michael Weinreich, PhD, Van Andel Research Institute, 333 Bostwick Ave. NE, Grand Rapids, MI 49503, USA.
E-mail: michael.weinreich@vai.org

Received 14 December 2016; Revised 10 March 2017; Accepted 13 March 2017



1476-5586
http://dx.doi.org/10.1016/j.neo.2017.03.001

kinase activity and targeting to various substrates [3]. Both DDK subunits are overexpressed in many primary tumors and in the majority of tumor cell lines tested [4–7]. Overexpression of DDK is correlated with poor prognosis and advanced tumor grade in melanoma, ovarian, breast, and other cancers [4–7]. High levels of DDK, however, are not correlated with increased proliferative capacity in tumor cell lines [4]. It is therefore not clear what survival advantage, if any, high DDK levels confer on tumors. In addition to its essential role in initiating DNA replication, DDK also has important functions in mediating replication checkpoint signaling [8,9], translesion DNA repair [10,11], and mitotic [12] and meiotic phases of cell cycle [13]. Most recently, we have identified a primary role for DDK in processing stalled replication forks and initiating replication checkpoint signaling (unpublished data). We found that DDK activity is also required for the efficient restart of forks once the replication stress or damage has been repaired. It is therefore conceivable that tumor cells rely on these functions of DDK to cope with increased genomic instability and replication stress.

Within the last decade, DDK has emerged as a possible chemotherapeutic target. Depleting CDC7 kinase or inhibiting DDK activity induces apoptosis in tumor cells, while normal cells undergo a reversible cell cycle arrest [14–16]. A detailed study of the reversible cell cycle arrest induced in normal fibroblast cells uncovered three nonredundant G1-S signaling pathways that inhibit CDK and/or Myc activity when DDK is inhibited, thus restricting progression into S-phase [16]. Since one or more of these growth suppressors are commonly disrupted in tumor cells, they can progress through a lethal cell cycle in the absence of DDK. The apoptosis of tumor cells upon DDK inhibition might involve ATR but is independent of the downstream canonical S-phase checkpoint kinases like CHK1 and CHK2 [14,15]. Apoptosis is also independent of p53 activity, although p53 status might influence the timing of apoptosis [14,17]. It is therefore not clear mechanistically how DDK inhibition induces cell death. A better understanding of this pathway is needed to identify tumors that would respond best to DDK inhibition and to uncover mechanisms through which tumors might become resistant to DDK inhibitors. In this study we have addressed how tumors increase DDK levels and how they might benefit from high DDK expression. We have also identified a number of kinases and phosphatases that mediate tumor cell death when DDK is inhibited.

Our results show that increased DDK expression correlates with tumor response to genotoxic insults and with increased resistance to genotoxic chemotherapy, which could explain the poor prognosis for patients with high DDK expressing tumors. Using The Cancer Genome Atlas (TCGA) mutation data, we also report a strong link between DDK expression and the tumor mutational load, strongly suggesting that DDK promotes mutagenesis. We also find that DDK expression is highly correlated with RB1 mutation and the "E2F-target" oncogenic signature, suggesting that E2F family members drive aberrant DDK expression in tumor cells. Using publicly available ChIP-Seq data, we show that several E2F family members tightly bind promoters at both *CDC7* and *DBF4* genes. Finally, using a functional RNAi screen of human kinases and phosphatases, we identify multiple mediators of cell death induced upon DDK inhibition. The LATS2 kinase is a novel tumor suppressor that promotes apoptosis when DDK is inhibited, and we find that its role may be independent of upstream Hippo signaling. Other top hits from the screen are required for mitotic progression, further strengthening a model where aberrant progression through mitosis in the absence of DDK triggers cell death.

## Results and Discussion

### *Gene Expression Signature of Tumors Differentially Expressing DDK Subunits*

Based on previous studies [8–10], we hypothesized that tumors with increased DDK expression are better able to activate a checkpoint or DNA repair pathway in response to genotoxic insults and as a result are more resistant to genotoxic chemotherapies. To test this hypothesis, we used the well-annotated lung adenocarcinoma dataset from TCGA [18]. We first compared the expression level of DDK in matched normal and tumor tissue. We found that all DDK subunit genes (*CDC7*, *DBF4*, and *DBF4B*) are significantly overexpressed in lung adenocarcinoma tumor tissue when compared to their matched normal tissue [$N$ = 57, $P$ values = $9.4 \times 10^{-10}$ (*CDC7*), $1.1 \times 10^{-16}$ (*DBF4*), $5.2 \times 10^{-13}$ (*DBF4b*) using the Kolmogorov-Smirnov test] (Supplementary Figure 1*A*). Moreover, patients with *CDC7*-overexpressing tumors have significantly worse survival (hazard ratio of 1.58, multivariate analysis $P$ value = .00326) (Supplementary Figure 1*B*). These results indicate that a high level of *CDC7* expression is independently prognostic of poor survival in lung adenocarcinoma, which is consistent with previous studies showing similar outcome for *CDC7* overexpression in other cancer types. It also suggests that DDK has a universal role in promoting tumor survival.

We then used gene expression data from the top 10 *CDC7*-high–expressing tumors and bottom 10 *CDC7*-low–expressing tumors to generate a gene expression signature correlated with *CDC7*. Genes with $Z$-scores > = +3 were selected as genes upregulated in *CDC7*-high–expressing tumors, and those with $Z$-scores < = −3 were selected as genes downregulated in *CDC7*-high–expressing tumors. The selected lists of genes were then queried for enriched gene sets using Gene Set Enrichment Analysis (GSEA). Among the genes positively correlated with high *CDC7* expression, we found several gene sets indicative of advanced tumor grade or poor prognosis (Supplementary Table 1). We also identified several cell cycle gene sets including (not surprisingly) those involved in DNA replication and activation of the prereplicative complex, which is the essential role of DDK (Supplementary Figure 2*A*). Several mitotic genes sets were also upregulated in *CDC7*-high–expressing tumors including the PLK1 pathway (Figure 1*A*), supporting the published data in yeast that DDK interacts with and inhibits Polo-like kinase to prevent mitotic progression [12,19]. Gene sets involved in the G2/M checkpoint, activation of the ATR pathway, and response to HU damage were also significantly enriched. These latter gene sets corroborate our recent finding that DDK is involved in processing stalled replication forks and in initiating the DNA replication checkpoint (our unpublished data).

Lastly, chemoresistance gene sets were also significantly enriched in *CDC7*-high–expressing tumors (Figure 1*A*). The positive correlation of high DDK expression with increased chemoresistance offers an explanation for the poor survival outcome in these patients. Expression of mitotic and G2/M checkpoint genes is enriched in cisplatin-resistant lung adenocarcinoma mouse models [20] as in *CDC7*-high–expressing tumors. Furthermore, since *CDC7* and *MCM7* (MCM7 is a direct target of DDK) were among the top genes overexpressed in a cisplatin-resistant bladder cancer cell line [21,22], perhaps DDK plays a direct role in generating cisplatin resistance. In budding yeast, DDK promotes replication initiation by phosphorylating the Mcm4 and Mcm6 proteins [23]. But Mcm7 was among the most potent DDK targets *in vitro*, and *mcm7-1* exhibited deleterious genetic interactions with *cdc7* and *dbf4* hypomorphic mutants [22]. The significance of DDK phosphorylation of MCM7 is not understood, but it is possible that MCM7 phosphorylation is important for the response to genotoxins such as cisplatin or for the maintenance of genome stability in tumor cells.

**A**

Cell cycle checkpoint and drug resistance pathways enriched in CDC7-high expressing tumors

| Curated Gene Sets | Brief Description | FDR q-val |
|---|---|---|
| REACTOME_CELL_CYCLE_CHECKPOINTS | Genes involved in Cell Cycle Checkpoints | 0 |
| HU_GENOTOXIC_DAMAGE_4HR | Genes most consistently regulated at 4 h by all six genotoxins tested: cisplatin, methyl methanesulfonate, mitomycin C, taxol, hydroxyurea and etoposide. | 0 |
| REACTOME_ACTIVATION_OF_ATR_IN_RESPONSE_TO_REPLICATION_STRESS | Genes involved in Activation of ATR in response to replication stress | 0 |
| REACTOME_CHROMOSOME_MAINTENANCE | Genes involved in Chromosome Maintenance | 0 |
| REACTOME_G2_M_CHECKPOINTS | Genes involved in G2/M Checkpoints | 0 |
| KANG_DOXORUBICIN_RESISTANCE_UP | Genes up-regulated in gastric cancer cell lines: doxorubicin resistant vs. sensitive | 0 |
| PID_PLK1_PATHWAY | PLK1 signaling events | 0 |

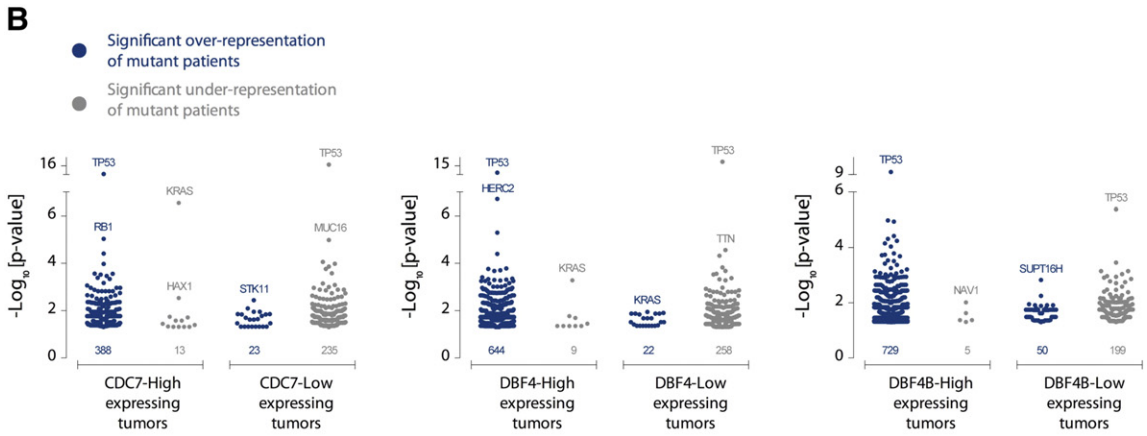


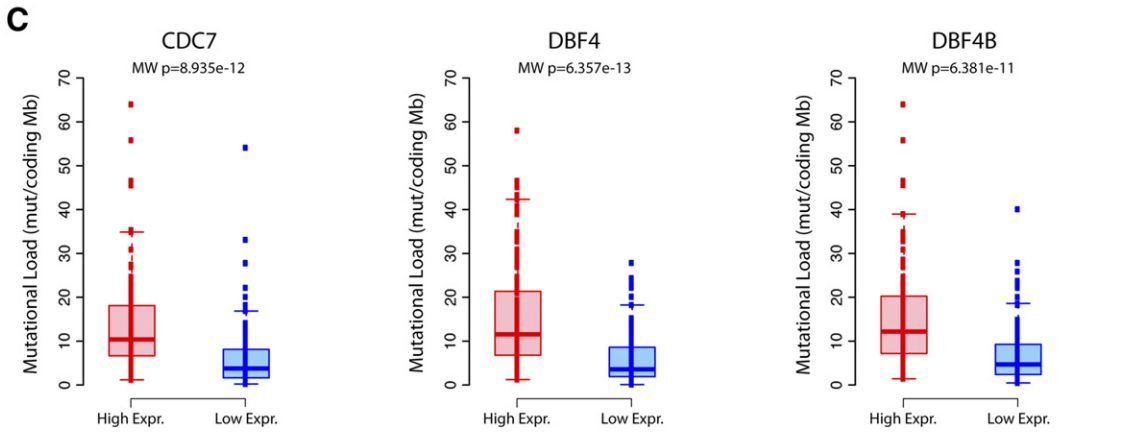


**Figure 1.** Characterization of tumors that differentially express DDK. (A) GSEA was performed using a gene expression signature differentiating CDC7-high versus CDC7-low tumors. Shown here are enriched gene sets involved in cell cycle checkpoints and drug resistance. (B) Genes with overrepresentation of mutant patients within patients groups that differentially express DDK subunits. Mutational information from the top and bottom 25% of CDC7/DBF4/DBF4B-expressing tumors was used to assess significant ($P < .05$, hypergeometric test) overrepresentation (blue) or underrepresentation (gray) of mutant patients. The number under each data set indicates the total number of genes with significant over- or underrepresentation of mutant patients within each cohort. (C) Mutational load (derived as the number of nonsilent mutations per 30 Mb of coding sequence) in patients with high CDC7/DBF4/DBF4B expression (top 25%, $n = 122$) and low CDC7/DBF4/DBF4B expression (bottom 25%, $n = 122$). Mann-Whitney-Wilcoxon (MW) test was used to assess statistical significance.

### *DDK Drives Increased Tumor Mutagenesis*

To investigate how DDK might contribute to tumorigenesis, we examined the mutation spectrum of *CDC7*-, *DBF4*-, and *DBF4B*-high–versus -low–expressing tumors. The top 25% and bottom 25% ($n = 122$) of patients were selected based on *CDC7*, *DBF4*, or *DBF4B* expression. Overrepresentation of patients with mutations in specific genes within each group was assessed with respect to the background rate in the whole cohort (hypergeometric test) (Supplementary Table 1). The group of patients that had tumors with high levels of DDK expression exhibited significantly increased mutational load in a large number of genes

(*CDC7* = 388; *DBF4* = 644; *DBF4B* = 729), whereas only a handful of genes in these patients exhibited mutation rates lower than those expected by chance (*CDC7* = 13, *DBF4* = 9, *DBF4B* = 5) (Figure 1*B*). Surprisingly, very few genes had significantly increased rates of mutation in patients that had tumors with low levels of DDK expression (*CDC7* = 23; *DBF4* = 22; *DBF4B* = 50). In contrast, in this low–DDK expression group, several hundred genes had mutation rates significantly *lower* than what is expected by chance (*CDC7* = 235; *DBF4* = 258; *DBF4B* = 199) (Figure 1*B*). It is possible that a few patients with very high mutational load in the DDK-high group might be driving this difference. To directly test this possibility, we compared the mutational load, measured as the number of mutations per Mb of the coding DNA, between the two groups of patients with high and low expression of DDK subunits. We again found significantly higher mutational load in tumor patients that overexpress all three DDK subunits using this test (Figure 1*C*), ruling out the possibility that a few patient samples were skewing the results. Together, these analyses suggest that DDK is a driver of tumor mutagenesis.

A positive correlation between DDK expression and the mutational load could be indicative of the improved ability of tumor cells to tolerate genome instability, which is a known mechanism for increased mutation rate in tumor cells [2]. This mechanism, however, does not explain why patients with "DDK-low"–expressing tumors are significantly underrepresented in mutational load for such a large number of genes. In the budding yeast, DDK promotes error-prone repair and UV/MMS-induced mutagenesis. Yeast strains containing hypomorphic *cdc7* alleles are almost immutable in response to these mutagens [24,25]. Moreover, yeast strains harboring multiple copies of the wild-type *CDC7* gene exhibited increased rate of UV-induced mutagenesis [26]. Subsequently, it was found that *CDC7* has an epistatic relationship with genes that promote an error-prone DNA repair mechanism known as the translesion DNA synthesis [11,27]. In human cell lines, DDK phosphorylates the RAD18 ubiquitin ligase, which is important for the recruitment of translesion DNA synthesis polymerase η to replication stall sites [10]. Therefore, DDK has a likely conserved role to promote error-prone DNA synthesis, which could be one of the mechanisms for increased mutagenesis in DDK-high–expressing tumors. Our finding is the first report that mutational load is strongly correlated with DDK expression in humans and has potentially important chemotherapeutic implications. That is, inhibiting DDK activity in tumor cells (in addition to promoting tumor cell death) might reduce acquisition of new mutations that would otherwise help promote resistance against chemotherapeutic drugs.

### *RB1 Mutation is Strongly Correlated with High DDK Expression in Tumors*

The RB1-E2F pathway genes formed a significant subset of gene sets that were positively correlated with high *CDC7* expression (Supplementary Figure 2*B*). The expression signature of *CDC7*-high–expressing tumors was similar to the oncogenic signature of the RB1-E2F pathway (Supplementary Figure 2*C*). RB1 is a tumor suppressor that controls the expression of hundreds of genes, especially those involved in G1/S progression. RB1 binds and sequesters the E2F family of transcription factors in G1 phase. In late G1, CDKs hyperphosphorylate RB1, which leads to the release of E2F transcription factors and increased expression of genes required for the G1/S transition and S phase progression [28]. RB1 is frequently mutated in certain tumors, with highest rates of mutation in retinoblastoma, osteosarcoma, and small-cell lung cancers [28]. RB1 mutations are often inactivating but could also increase the phosphorylation of RB1 [28]. In addition, E2F gene loci are amplified and have increased protein expression levels in several cancers [29]. Therefore, a strong correlation between high *CDC7* expression and E2F pathway genes could be caused by mutation of RB1 or other pathways that activate the E2F family of transcription factors.

We first tested if RB1 mutation is correlated with high or low DDK expression. Mutational Signature analysis (using MutSig) of tumors from the top-10 *CDC7*-high–expressing patients showed that RB1 was among the most recurrently mutated genes (Supplementary Figure 3*B*). We then directly tested for the overrepresentation of RB1 mutant patients within the high– and low–DDK expression patient groups (hypergeometric test). RB1 had significantly increased rate of mutation in patients with tumors that express high levels of *CDC7*, *DBF4*, or *DBF4B* (Supplementary Figure 3*C*, Figure 1*B*). There was no significant correlation between RB1 mutation and the low–*CDC7* expression group. As shown previously, DDK expression levels were also strongly correlated with mutations in p53 [4] (Figure 1*B*, Supplementary Figure 3*C*). These data strongly suggest that RB1-E2F promotes the expression of DDK in tumor cells. We queried whether E2F family members bind to the *CDC7* or *DBF4* promoter using publicly available ChIP-Seq datasets. We first searched for E2F transcription factor binding at *CDC7* or *DBF4* promoter sites using ENCODE-annotated data. Binding of E2F transcription factors at their well-known target gene *MCM4* is shown as positive controls (Figure 2C). E2F1, E2F4, and E2F6 transcription factors showed very tight binding at *CDC7* and *DBF4* promoter regions (Figure 2, *A* and *B*). This finding was verified by E2F ChIP-Seq from multiple cancer cell lines (Supplementary Figure 3*D*). Moreover, analysis of raw ChIP-Seq data also showed binding of E2F3 at *CDC7* and *DBF4* promoter sites [30,31]. Binding by E2F1/F3 activators and E2F4/F6 repressors to the same promoter could reflect the fact that different cell cycle phases are represented in an asynchronous cell population and that E2F target promoters can be occupied by different E2Fs in a cell cycle–dependent manner [32]. A previous report showed that E2F1, 2, and 3 bound to the human *DBF4* promoter and promoted *DBF4* expression in an atypical manner that was independent of consensus E2F-binding sites [33]. Our RB1 mutational and E2F ChIP-Seq data are evidence that *both CDC7* expression and *DBF4* expression are driven by E2F family members and can explain why RB1 mutations are so strongly correlated with high DDK expression.

### *RNAi Screen Identifies Mediators of Apoptosis Following DDK Inhibition*

Preclinical studies in human cell lines and murine models have demonstrated the therapeutic potential of inhibiting DDK in tumor cells [14,15]. DDK inhibition causes a reversible G1/S cell cycle arrest in normal cells but induces apoptosis in many diverse types of tumors cells through an unknown signaling pathway. Apoptosis is not accompanied by CHK1 and CHK2 kinase activation, which can signal cell death when lethal amounts of DNA damage or irreversible replication fork arrest occur. The apoptotic response also occurs independently of p53 status. These results suggest that a novel apoptotic pathway is engaged upon DDK inhibition.

To identify mediators of this pathway, we used an RNAi screen against all human kinases and phosphatases to test their involvement in cell death upon DDK inhibition. We used the small molecule DDK inhibitor PHA-767491 (DDKi) to inhibit DDK activity in the HCC1954 breast cancer cell line. This inhibitor was chosen because it is a prototypical DDK inhibitor and has been shown to inhibit DDK and

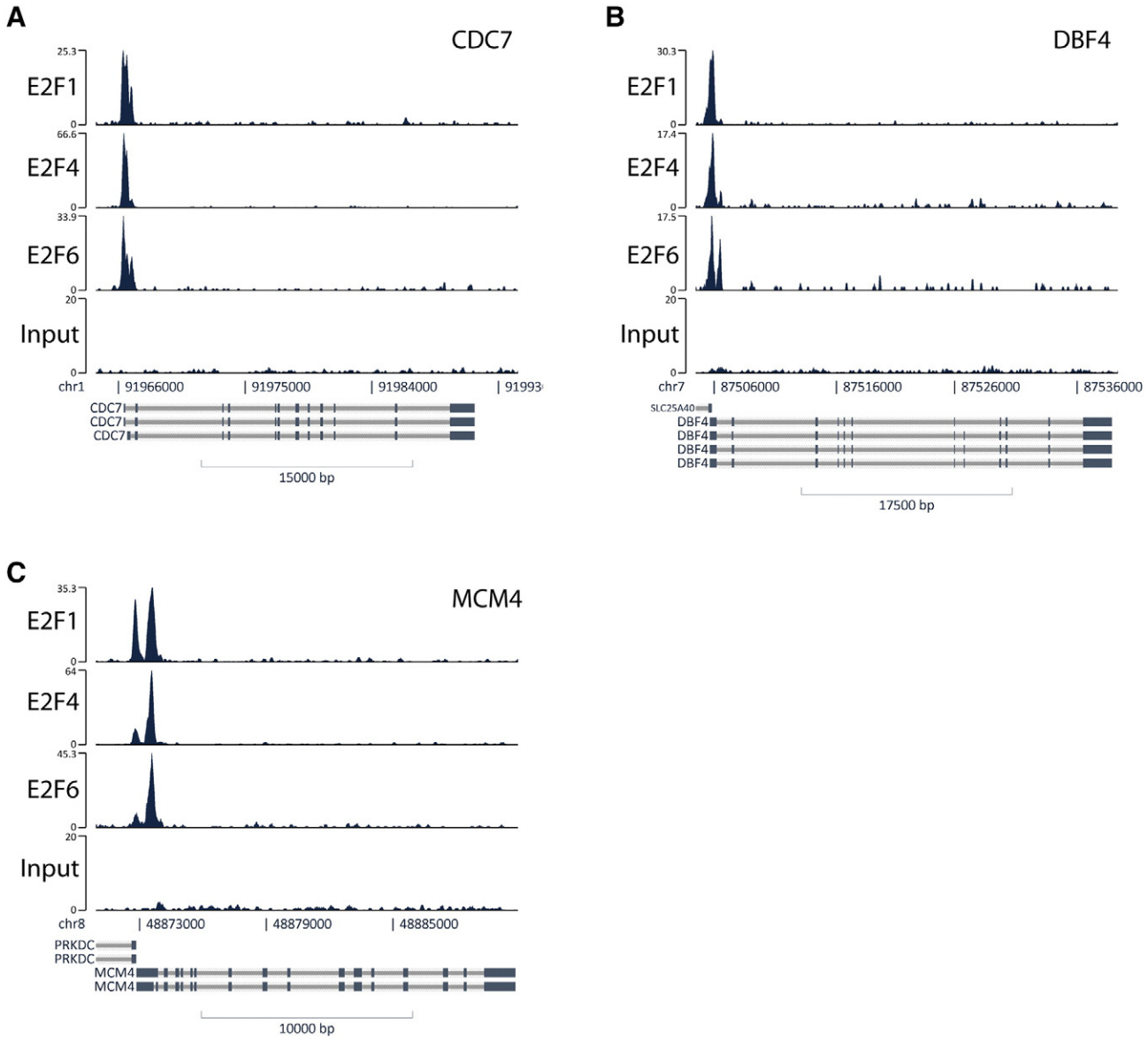


**Figure 2.** E2F family of transcription factors strongly bind DDK promoters. The HeLa-S3 ChIP-Seq data were obtained from ENCODE database and E2F binding analyzed using EaSeq software. (A, B, C). E2F ChIP-Seq signal intensities at the promoter regions of CDC7 (A), DBF4 (B), and MCM4 (C).

induce apoptosis in multiple cells lines and in preclinical cancer models. Although PHA-767491 has an off-target effect to inhibit CDK9 in cells, the strong apoptotic response induced by this compound depends on its ability to inhibit DDK. While other off-target effects of PHA-767491 were reported on several additional purified kinases, inhibition was seen using concentrations 100-fold above the 10-nM $IC_{50}$ concentration that inhibits purified DDK, and has not shown to be relevant *in vivo*. A more selective XL413 inhibitor against purified DDK has the significant drawback of limited bioavailability in multiple cancer cell lines [34] and so was not used here. The HCC1954 cell line was selected for our analysis from a panel of breast cancer cell lines that express high levels of DDK [34] based on its reproducible and robust apoptotic response to the DDKi. HCC1954 cells also induce a robust apoptotic response to *CDC7* knockdown using different single siRNAs (data not shown), which further confirms that this cell line induces apoptosis in response to DDK inhibition.

HCC1954 cells were transfected with pooled siRNAs against individual kinases and phosphatases followed by the addition of DDKi (Figure 3) and measurement of cell viability after 72 hours. We screened for instances where knockdown of a target gene prevented the loss of viability induced upon DDK inhibition. The screen was performed in duplicate and was highly reproducible (Figure 3*A*). The primary screen resulted in 56 hits with a robust *Z*-score ≥ 2 and 17 hits with *Z*-scores ≤ −2 (Supplementary Table 2), i.e., 2 SDs above (or below) the median cell viability measurement. Hits with positive *Z*-scores (potential mediators of cell death) were ranked using three separate gene ranking software to narrow the list to 41 hits (Figure 3*C*) (also see experimental procedures). All hits with robust *Z*-score greater than 3 were included in our list of 41 genes for further analysis regardless of this secondary ranking. These 41 hits were then rescreened in secondary assays with deconvoluted sets of siRNA (4 individual siRNAs per gene) using an assay similar to the primary screen. We then used an

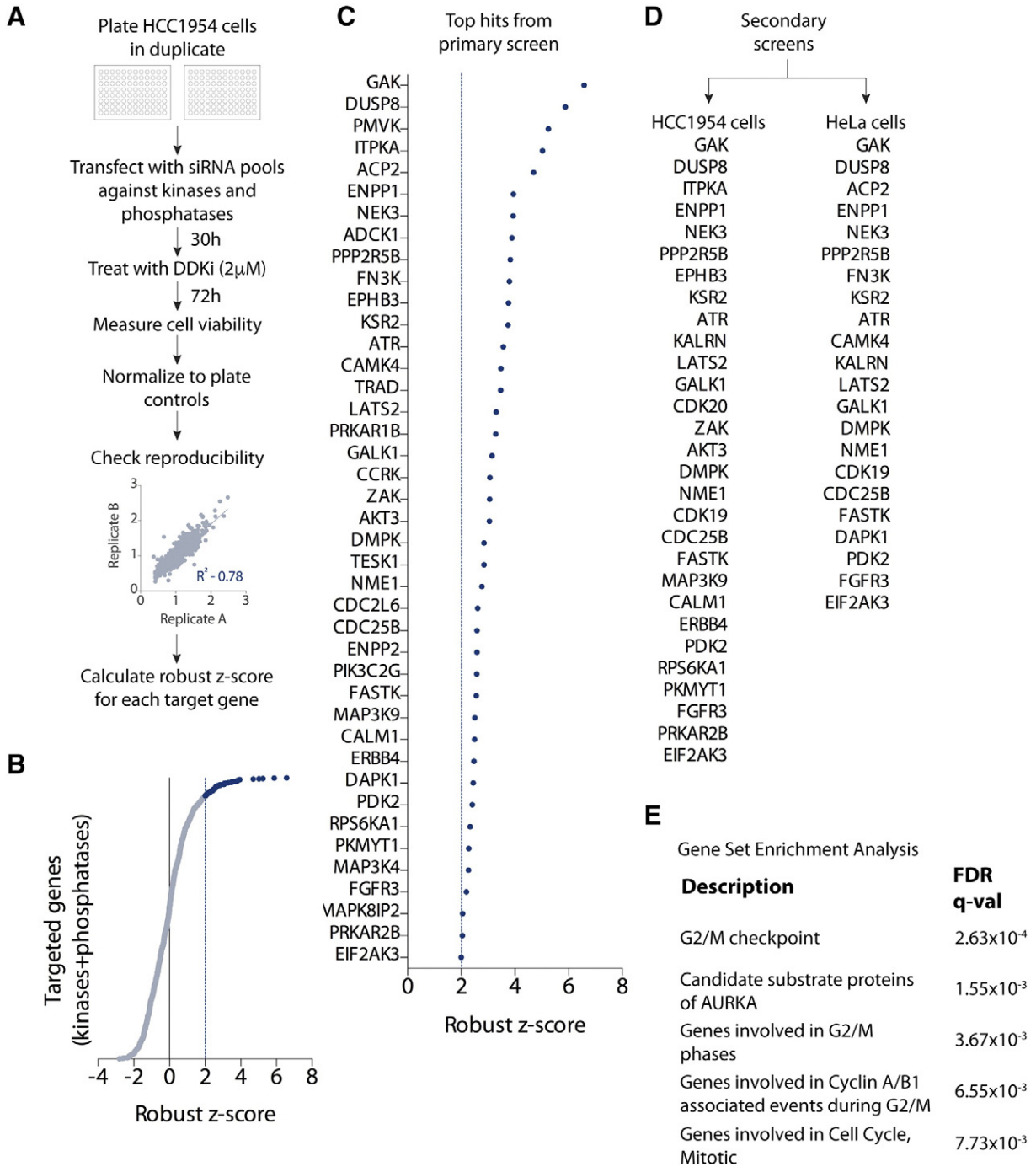


**Figure 3.** RNAi screen to identify mediators of cell death induced upon DDK inhibition. (A) Outline of the RNAi screen. (B) Scatter plot of all targeted genes. Hits with robust Z scores > = 2 are highlighted in blue. (C) List of top 41 hits from the primary screen. (D) Hits validated by secondary screens in HCC1954 cells or HeLa cells. (E) G2/M and mitotic gene sets enriched in hits validated in (D).

alternate readout for cell death by directly measuring the Caspase 3/7 activity of the cell. In this secondary screen in HCC1954 cells, we confirmed 29 of the 41 hits from the primary screen (Figure 3*D*, Supplementary Figure 5). Finally, we also screened the 41 hits in the independent HeLa cervical cancer cell line for their ability to mediate cell death in response to DDKi. Of the 41 targets tested, we identified 23 genes whose knockdown in HeLa cells also prevented the loss of viability induced upon DDK inhibition (Figure 3*D*, Supplementary Figure 6). Therefore, we identified multiple potential mediators of the cell death pathway induced upon DDK inhibition. We point out that an earlier study identified the stress kinase p38 mitogen-activated protein kinase as required for apoptosis following *CDC7* siRNA-mediated knockdown in HeLa cells [35]. We did not identify p38 in our initial RNAi screen in HCC1954 cells, but we carried it forward as a hit nonetheless in the secondary screens. The p38 knockdown did not rescue cell death in the HCC1954 in the secondary screen or in the HeLa cell line. We were also not able to see p38 rescue of apoptosis in HeLa cells using an siRNA to knockdown *CDC7*. We cannot explain this discrepancy, although another group also found that p38 inhibition did not prevent DDKi-induced apoptosis in HeLa cells but instead they

found that p38 inhibition actually *enhanced* apoptosis following DDK inhibition (using PHA-767491) in multiple myeloma cancer cell lines (C. Santocanale, personal communication).

We identified a small set of genes whose knockdown exacerbated the cell death upon DDK inhibition (Supplementary Table 2, hits with *Z*-scores <= −2). While knocking down some of these genes could result in cell death regardless of DDK inhibition, others might sensitize tumors cells to DDK inhibition. The hits included genes essential for cell growth and division like *CSNK1D*, *CKS1B*, *SRC*, *ERBB2*, and *JAK2*. The top hit, *PPP2R2B* (PP2A-B55β), encodes an isoform of the protein phosphatase 2A (PP2A)-B55 holoenzyme. In fission yeast, *Drosophila*, *Xenopus*, and mammalian cell PP2A-B55 phosphatase inhibits mitotic entry by dephosphorylating both CDC25 phosphatase (thereby inactivating it) and WEE1 kinase (activating it) [36–38]. Inactive CDC25 phosphatase and active WEE1 kinase result in persistent inhibitory phosphorylation of CDK and inhibition of mitotic entry. Therefore, aberrant entry into mitosis might sensitize tumors cells to DDK inhibition. A similar strategy of forced mitotic entry was recently shown to increase tumor sensitivity to ATR inhibitors [39].

### *Enrichment of Mitotic Mediators in siRNA Hits*

To identify potential shared pathways, we used the 29 confirmed hits in HCC1954 cells (Figure 3*D*) and performed a GSEA (Figure 3*E*, Supplementary Figure 7). Due to the inherent bias in the screen (only kinases and phosphatases were targeted), this analysis was not very powerful. Despite this limitation, we found that several proteins required for efficient mitotic progression were enriched in our data set (Figure 3*E*). The top hit in our screen was Cyclin G associated kinase (GAK). It has important roles in centrosome maturation, chromosome segregation, and clathrin-mediated membrane trafficking [40,41]. GAK phosphorylates and increases the activity of PP2A-B56 holoenzyme (related to PP2A-B55 mentioned above), which is required for mitotic progression [41]. Importantly, RNAi-mediated knockdown of GAK induces cell cycle arrest at metaphase and activation of the spindle assembly checkpoint [40]. Interestingly, we also identified a component of the PP2A-B56 holoenzyme in our screen, PPP2R5B (Figure 3, *C* and *D*). PP2A holoenzyme is composed of a catalytic subunit (PPP2CA-B), a regulatory subunit (PPP2R1A), and a substrate targeting subunit (PPP2R5A-E). PP2A-B56 is essential for proper chromosome alignment during metaphase, for activation of anaphase-promoting complex, and therefore for mitotic progression [42,43]. Another recent finding using budding yeast has shown that PP2A-B56 yeast homolog (Rts1) could be redundant with CDC25 phosphatase in promoting entry into mitosis by dephosphorylating CDK1 [44]. CDC25B phosphatase was also identified in our screen (Figure 3, *C* and *D*). Taken together, these hits affecting mitotic regulators strongly suggest that preventing mitotic progression upon DDK inhibition can protect against cell death.

Several hits with positive *Z*-scores (potential mediators of cell death) are known to be involved in apoptosis or stress response pathways. NME1 is one of only two known mammalian protein histidine kinases [45]. NME1 (also known as NM23-H1 or nucleotide diphosphate kinase) is involved in cellular nucleotide triphosphate homeostasis and was the first identified metastasis suppressor gene [45]. It is also required for maintaining genomic stability, cytokinesis [46], and UV-induced DNA repair [47]. Given that DDK also maintains genome stability and regulates error-prone repair of UV lesions, NME1 is a potentially interesting mediator of cell death upon DDK inhibition. Knockdown of *MAP3K9* also led to rescue of DDKi-mediated cell death. Somatic inactivating mutations in *MAP3K9* are common in metastatic melanomas and also result in increased chemoresistance [48].

### *LATS2 Kinase Mediates Cell Death upon DDK Inhibition*

LATS2 kinase, a Hippo signaling component, was among the top positive *Z*-score hits identified in our siRNA screen. LATS1 and LATS2 kinases are functionally related tumor suppressors involved in mediating growth inhibitory signals in response to a variety of upstream cues [49]. Both kinases, however, also have roles independent of each other [50]. *LATS1* was not recovered in our screen, and *LATS1* knockdown did not rescue cell death upon DDK inhibition (Figure 4, *A* and *B*). We confirmed the role of LATS2 kinase in mediating cell death upon DDK inhibition using four separate siRNAs against *LATS2* (Figure 4, *A* and *B*). Given that LATS2 antibodies cross-react with LATS1 (Supplementary Figure 8*A*), we simultaneously knocked down LATS1 to better visualize LATS2 on the immunoblots [49]. LATS1 knockdown by itself had very little effect on DDKi-induced apoptosis (Figure 4*A*). The extent of apoptotic rescue seen with *LATS2* siRNAs exactly correlated with their knockdown efficiencies, with siRNA#1 showing the strongest knockdown as well as the strongest rescue phenotype (Figure 4, *A* and *B*). Knockdown of *LATS1* was not necessary to see the rescue of apoptosis by knockdown of *LATS2* (Supplementary Figure 8*B*). Because the DDK inhibitor used to induce cell death could have off-target effects, we independently confirmed that LATS2 mediated cell death in response to DDK inhibition following siRNA-mediated knockdown of *CDC7*. *LATS2* knockdown was able to rescue cell death induced by *CDC7* siRNA as seen by the rescue of PARP cleavage (Figure 4*C*). *LATS1* knockdown had only a minimal effect on PARP cleavage compared to the *LATS2* knockdown (Figure 4*D*). We then tested if the upstream kinases involved in the Hippo pathway have a role in DDK-mediated apoptosis. MST1 and MST2 are human orthologs of the *Drosophila* Hippo kinase [49]. These two kinases phosphorylate and activate LATS1/LATS2 kinases. Knockdown of *MST1*, *MST2*, or both did not prevent DDKi-induced cell death (Figure 4*E*), and neither gene was identified in our screen. A recent study has found that MST1 and MST2 are not absolutely essential for activation of LATS1/LATS2 [51] and that MAP4K1/2/3 and MAP4K4/6/7 can together activate LATS1/LATS2 in parallel with MST1/MST2 [51]. However, knockout of all six MAP4Ks along with MST1/2 was required to see a near-complete abrogation of LATS activation [51]. Although none of the individual MAP4Ks were identified in our screen, it remains to be seen if multiple MAP4K family members cooperate to activate LATS2 following DDK inhibition. Taken together, our data show that LATS2 is required to promote apoptosis in response to DDK inhibition, but its upstream signaling kinase is unknown.

The principal downstream target of the LATS1 and LATS2 kinases is the transcription factor YAP. Phosphorylation of YAP by LATS1 or LATS2 causes it to be sequestered in the cytoplasm and/or degraded by the proteasome [49]. As a surrogate for basal LATS2 activity, we looked at a canonical YAP phosphorylation site S127 (pYAP S127). Two renal cancer cell lines, 786-O and ACHN, have inactivating deletions in the Hippo signaling gene *SAV1*, and SAV1 acts together with MST1/MST2 upstream of LATS2 kinase [52]. We reasoned that these cell lines would therefore have reduced basal levels of LATS2 activity. We probed 786-O and ACHN cells for pYAP S127 levels and found that S127 phosphorylation was significantly reduced compared to HCC1954 cells (Figure 4*F*). Therefore, these cell lines likely also have reduced basal LATS2 activity and therefore might be resistant to DDK inhibition. We found that both 786-O and ACHN cells had significantly lower rate of

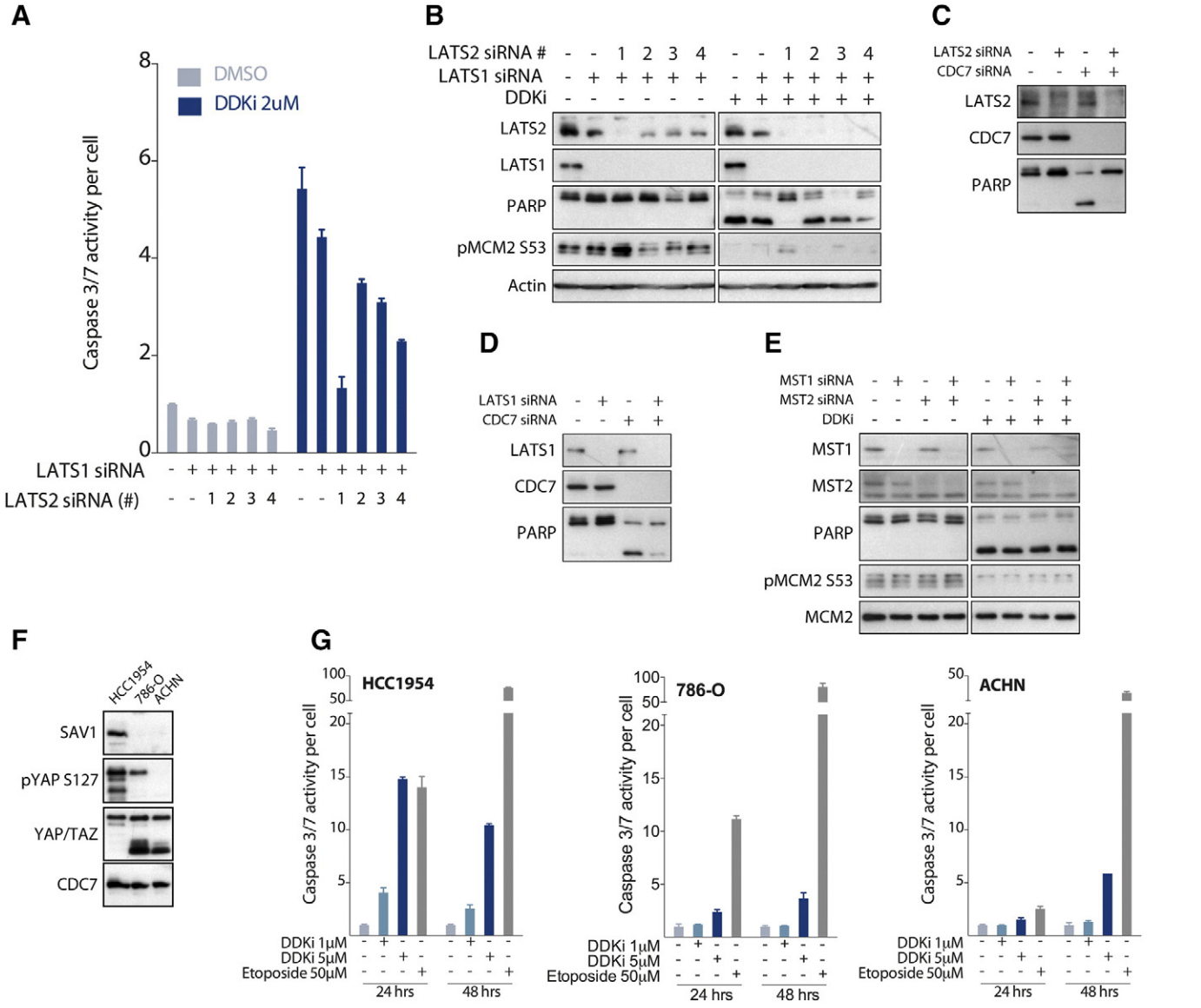


**Figure 4.** LATS2 mediates cell death upon DDK inhibition. (A, B) HCC1954 cells were transfected with the indicated siRNAs, 48 hours later treated with DDKi for 8 h, and harvested for Caspase 3/7 analysis (A) or Western blot (B). (C, D) HCC1954 cells were transfected with the indicated siRNAs and 72 hours later harvested for Western blot. (E) HCC1954 cells were transfected with the indicated siRNAs, 48 hours later treated with DDKi for 8 hours, and harvested for Western blot. (F) Subconfluent population of HCC1954, 786-O, and ACHN was harvested and subject to Western blot. (G) HCC1954, 786-O, and ACHN cells were plated in 96-well plates and treated with indicated drugs, and Caspase3/7 activity was measured at indicated times.

cell death (Caspase 3/7 activation) in response to DDK inhibition when compared to the HCC1954 cells (Figure 4*G*). This was not due to a generalized defect in promoting apoptosis as all three cell lines were equally capable of undergoing apoptosis in response to etoposide, a topoisomerase inhibitor that induces dsDNA breaks and cell death (Figure 4*G*).

In summary, LATS2 kinase promotes cell death downstream of DDK inhibition, but this function may be independent of its canonical role in the Hippo signaling pathway. Interestingly, Hippo signaling has previously been shown to induce apoptosis under conditions of stress, and LATS2 can promote apoptosis through p53 stabilization and in polyploid cells [53]. Since LATS2 kinase promotes apoptosis in both breast cancer (HCC1954) and cervical cancer (HeLa) cell lines, which are both p53-deficient cells, the mechanism of apoptotic induction is likely mediated through a target different from p53. Given that ATR is activated and required for apoptosis in response to DDKi (Figure 3, *C* and *D* and unpublished data), it is tempting to speculate that ATR may directly phosphorylate LATS2 and promote this activity since the MST1, MST2, and mitogen-activated protein kinase 4 kinases are not required for apoptosis. Indeed, there are multiple [ST]Q sites in the C-terminus of LATS2 that could be phosphorylated by ATR. Moreover, LATS1 kinase was identified as a potential substrate of ATR/ATM kinase in a genome-wide screen for ATR/ATM target proteins [54]. Further studies will be required to understand how LATS2 kinase is activated in response to DDKi and how LATS2 alters the normal apoptotic response in response to DDK inhibition. Nonetheless, our study provides a wealth of possible apoptotic mediators in response to DDK inhibition that can now be further characterized, related to each other, and investigated mechanistically.

## Materials and Methods

### *Computational Data Analysis*

RNA-seq gene expression profiles of primary tumors and relevant clinical data of 488 lung adenocarcinoma patients were obtained from TCGA (TCGA LUAD; cancergenome.nih.gov). The Cox proportional hazards regression model was used to analyze the prognostic value of the *CDC7*, *DBF4*, and *DBF4B* expression across all patients within the TCGA LUAD cohort, in the context of additional clinical covariates. All univariate and multivariable analyses were conducted within a 5-year survival timeframe. The following patient and tumor-stage clinical characteristics were used: gene expression (*CDC7*, *DBF4*, *DBF4B*; log2, continuous); gender (male versus female); age (years, continuous); smoking history (reformed >15 years versus nonsmoker, reformed <15 years versus nonsmoker, current smoker versus nonsmoker); mutational load (derived as the number of nonsilent mutations per 30 Mb of coding sequence, continuous); Union for International Cancer Control (UICC) TNM stage specification (stage III/IV versus I/II); UICC T score specification (T2 versus T1, T3/T4 versus T1); and UICC N score specification (N1/N2 versus N0). Hazard ratio proportionality assumptions for the Cox regression model were validated by testing for all interactions simultaneously ($P$ = .2453). Interaction between *CDC7* expression and TNM stage, T score, and N score (significant covariates in the model) was tested using a likelihood ratio test to contrast a model consisting of both covariates with another model consisting of both covariates plus an interaction term. No statistically significant difference was found between the two models (TNM: $P$ =.6878, T score: $P$ = .4766, N score: $P$ = .5044; likelihood ratio test).

Empirical cumulative distribution function plots were generated to compare gene expression levels across matched normal and tumor samples ($n$ = 57) in the TCGA LUAD cohort. Standardized ($Z$-scores) gene expression values across normal and tumor samples were used, and the Kolmogorov-Smirnov (KS) test was used to assess statistical significance. The Mann-Whitney-Wilcoxon test was used to assess statistically significant differences in mutational load between patients with high *CDC7* (alternatively *DBF4*, *DBF4B*) expression (top 25%, $n$ = 122) and low *CDC7* (alternatively *DBF4*, *DBF4B*) expression (bottom 25%, $n$ = 122).

MutSig [55] was used to identify recurrently mutated genes within the *CDC7*-high– and -low–expression patient groups ($n$ = 122) with respect to the background mutational rate in covariate space. Additionally, the statistical significance of patients with mutations in a given gene represented within each of the high- and low-expression groups was assessed using the hypergeometric test (with the total of all patients in the cohort assessed for mutations as the universe). Similar analyses were conducted for patient groups with high and low *DBF4* and *DBF4B* expression. False discovery rate correction was performed for genes identified as belonging to a high-expression cluster in purity-filtered lung adenocarcinoma samples [56].

A gene expression signature comprised of differentially expressed genes between patients in the highest *CDC7* expression group ($n$ = 10) compared to those in the lowest expression group ($n$ = 10) was derived using a blind source separation strategy (based on independent component analysis) described earlier [57,58]. The R implementation of the core JADE algorithm (Joint Approximate Diagonalization of Eigenmatrices) [59–61] was used along with custom R utilities. Subsequent enrichment analyses were performed using GSEA [62] and MSigDB [63]. GSEA and Ingenuity Pathway Analysis (QIAGEN, Redwood City, CA) were used for enrichment analyses of targets assessed from RNAi screens.

All statistical analyses were conducted in R (www.R-project.org), and all survival analyses were conducted using the survival package in R.

### *ChIP-seq Data Analysis*

HeLa-S3 ChIP-seq data for E2F1, E2F4, E2F6, and input were downloaded from the ENCODE website under accession number ENCFF000XDA (E2F1), ENCFF000XDB (E2F4), ENCFF000XDH (E2F6), and FF459QXO (input). Data analysis and visualization were performed using EaSeq software [64] or Integrative Genomics Viewer [65].

### *Cell Lines and Reagents*

HCC1954 (ATCC), 786-0 (NCI-60), and ACHN (NCI-60) cells were cultured in RPMI-1640 media supplemented with 10% heat-inactivated FBS, 50 U/ml of penicillin, and 50 μg/ml of streptomycin. HeLa cells (ATCC) were cultured in MEM supplemented with Earle's salts, 2 mM glutamine, 10% heat-inactivated FBS, 1.5 g/l sodium bicarbonate, 0.1 mM nonessential amino acids, 1 mM sodium pyruvate, 50 U/ml of penicillin, and 50 μg/ml of streptomycin. The DDK inhibitor, PHA-767491, was synthesized as described previously [34]. Etoposide (#341205) was from EMD Millipore. The antibodies were purchased as indicated: CST: PARP (#9542), LATS1 (#3477), MST1 (#3682), MST2 (#3952), SAV1 (#13301), YAP/TAZ (#8418), pYAP S127 (#13008); Bethyl Laboratories Inc.: pMCM2 S53 (A300-756A), MCM2 (A300-122A), LATS2/LATS1 (A300-479A); MBL International Corporation: CDC7 (K0070-3S); Sigma: β-actin (A5441); GE Healthcare: anti-mouse-HRP (NA931V), and anti-rabbit-HRP (NA934V).

### *Primary RNAi Screen*

HCC1954 cells were plated in white-walled, white-bottom 96-well plates (2500/well) and allowed to grow for 24 hours before transfection. Forward transfection with 25 nM pooled-siRNA (4 siRNAs) was performed using Oligofectamine (Invitrogen, 2 μl/ml final concentration) in duplicate 96-well plates. Thirty hours after transfection, cells were treated with fresh media containing DMSO or 2 μM DDKi. Seventy-two hours later, growth media were removed and 50 μl of CellTiter-Glo (diluted 1:1 in phosphate-buffered saline at room temperature) was added to each well. Luminescence was measured using EnVision 2104 Multilabel Reader (PerkinElmer) 10 minutes after addition of "Glo" reagent. Three to six wells of negative control (cells transfected with nontargeting siRNA and treated with 2 μM DDKi), positive control (cells transfected with nontargeting siRNA and treated with 2 μM DDKi+ 50 μM caspase inhibitor zVAD), and transfection control (cells transfected with 25 nM ACDC siRNA) were included in each plate. Loss of viability in ACDC siRNA-treated wells (transfection control) was indicative of efficient transfection in each plate (Supplementary Figure 4*A*). Viability values from the positive and negative controls in each plate were used to calculate $Z'$-factor [66] (Supplementary Figure 4*B*). All plates had $Z'$-factor ~0.5 or above (Supplementary Figure 4*C*), which is indicative of a robust assay with wide separation between positive and negative control values. Raw luminescence values were normalized to the median of each plate (controls were excluded). The normalized values from each plate were subsequently used to calculate robust $Z$-scores as described previously [67]. An arbitrary threshold of $Z$-score > = + 2 or $Z$-scores <= – 2 was set for hit selection. Supplementary Table 2 lists all hits identified by this criterion. Only hits with positive $Z$-scores (potential mediators of cell

death) were considered for further analysis (56 hits, Supplementary Table 2). Gene ranking software GPSy [68], Endeavor [69], and ToppGene [70] were used to rank hits, and some of the low-ranking hits were removed from further analysis (Supplementary Table 2). All hits with *Z*-scores > = + 3 were included irrespective of their ranks. The final list of 41 genes is shown in Figure 3*C* and Supplementary Table 2.

### *Secondary RNAi Screen*

Using a library of 164 deconvoluted siRNAs (4 siRNAs against 41 hits), a secondary screen identical to the primary RNAi screen was performed in HCC1954 cells (Supplementary Figure 5). A second assay was performed in parallel using caspase 3/7 activity as a direct indicator of apoptosis. The time lines are shown in Supplementary Figure 5. Both assays were performed in duplicate and were highly reproducible (Supplementary Figure 5). The *Z'*-factor for each plate was calculated as described above (Supplementary Figure 4, *D* and *E*). *Z*-scores were calculated for each hit/siRNA, and an arbitrary threshold for hit selection was set for each assay as indicated (Supplementary Figure 5). Twenty-four (58.5%) of the 41 hits rescreened with at least 2 separate siRNAs. An additional set of five hits that rescreened with only one siRNA in *both* viability and apoptosis assays was also included in the final analysis. The list of 29 hits is shown in Figure 3*D*. Cell line–specific effects were tested by performing the secondary screen in HeLa cervical cancer cell line. The assay, outlined in Supplementary Figure 6, was performed similar to the secondary screen in HCC1954 cells. Due to higher cytotoxicity in HeLa cells, siRNAs were used at a final concentration of 10 nM instead of 25 nM used in HCC1954 cells. The *Z'*-factor for each plate was calculated as described above (Supplementary Figure 4, *F* and *G*). Twenty-three of the 41 hits rescreened with at least one siRNA, and the genes are listed in Figure 3*D*.

### *RNAi Interference*

Cells were plated in six-well plates (75,000 cells/well) and allowed to grow for 36 hours before transfection. siRNA transfection was performed with Lipofectamine RNAiMAX (Invitrogen) according to manufacturer's instructions. Each well was transfected with 2 µl of transfection reagent and a final siRNA concentration of 25 nM in a total volume of 2 ml. Media were replaced 24 hours after transfection, and the cells were either harvested or exposed to indicated treatments 48 hours after transfection. Following siRNAs were used: *CDC7* (CDC7-L1, Dharmacon custom siRNA, GGCAAGATAATGTCAT GGGA), *LATS1* (Qiagen, SI02223655), *LATS2 # 1* (Qiagen, SI02660154), *LATS2 # 2* (Qiagen, SI02660161), *LATS2 # 3* (Qiagen, SI02660168), *LATS2 # 4* (Qiagen, SI02660385), *MST1* (Qiagen, SI02622270), and *MST2* (Qiagen, SI02622256).

### *Immunoblotting*

Whole cell extracts were prepared by resuspending the pellets in RIPA buffer (150 mM NaCl, 1% NP-40, 0.5% sodium deoxycholate, 0.1% SDS, 50 mM Tris-HCl, pH 8) containing protease inhibitors (100 µM PMSF, 1 mM Benzamidine, 2.5 µg/ml Pepstatin A, 10 µg/ml Leupeptin, and 10 µg/ml Aprotinin) and phosphatase inhibitors (1 mM each of NaF, $Na_3VO_4$, and $Na_2P_2O_7$). Protein concentration was measured using the BCA protein assay kit (Pierce, #23227). Equal amounts of proteins were subjected to sodium dodecyl sulfate polyacrylamide gel electrophoresis and transferred to nitrocellulose membrane (Millipore, HATF304F0). Transfer efficiency and equal loading were confirmed by Ponceau S staining. Membranes were blocked overnight at 4°C with 5% nonfat milk in TBS-T, followed by incubation in primary and secondary antibodies (1 hour at RT, 2% milk in TBS-T). Protein bands were visualized using SuperSignal West Pico solutions (Thermo Scientific).

### *Analysis of Caspase 3/7 Activity*

For assays in 96-well plates, 5000 cells were plated per well. Twenty-four hours later, cells were treated and incubated for the indicated period of time at 37°C. Caspase 3/7 activity and viable cell number were then measured using the Caspase-Glo 3/7 assay (Promega) and CellTiter-Glo assay (Promega), respectively. For assays in six-well plates, cells were trypsinized, and a suspension was made in 1 ml of phosphate-buffered saline. Thirty microliters of this suspension was mixed with 30 µl of CellTiter-Glo, and another 30 µl was mixed with 30 µl of Caspase-Glo 3/7 reagent. The "caspase activity per cell" was obtained by normalizing total caspase activity to cell number. Luminescence was measured using BioTek Synergy Microplate Reader 30 minutes after addition of "Glo" reagents.

Supplementary data to this article can be found online at http://dx.doi.org/10.1016/j.neo.2017.03.001.

## Acknowledgements

We thank the NCI grant R01CA197398 (to J.P.M.), F32CA159709 (to N.J.L), NIH P01-CA042063 grant (to Phillip A. Sharp) and the NCI core center grant P30-CA14051 (for funding A.B.), the Van Andel Institute (M.W., N.K.S. and J.P.M.), and Michigan State University (N.K.S.) for supporting this work.

## References

[1] Hanahan D and Weinberg RA (2011). Hallmarks of cancer: the next generation. *Cell* **144**, 646–674.
[2] Jeggo PA, Pearl LH, and Carr AM (2016). DNA repair, genome stability and cancer: a historical perspective. *Nat Rev Cancer* **16**, 35–42.
[3] Sasi NK and Weinreich M (2016). In: Kaplan LD, editor. DNA Replication Checkpoint Signaling. Cham: Springer International Publishing; 2016. p. 479–502.
[4] Bonte D, Lindvall C, Liu H, Dykema K, Furge K, and Weinreich M (2008). Cdc7-Dbf4 kinase overexpression in multiple cancers and tumor cell lines is correlated with p53 inactivation. *Neoplasia* **10**, 920–931.
[5] Chen HJ, Zhu Z, Wang XL, Feng QL, Wu Q, Xu ZP, Wu J, Yu XF, Qian HL, and Lu Q (2013). Expression of huCdc7 in colorectal cancer. *World J Gastroenterol: WJG* **19**, 3130–3133.
[6] Cheng AN, Jiang SS, Fan CC, Lo YK, Kuo CY, Chen CH, Liu YL, Lee CC, Chen WS, Huang TS, et al (2013). Increased Cdc7 expression is a marker of oral squamous cell carcinoma and overexpression of Cdc7 contributes to the resistance to DNA-damaging agents. *Cancer Lett* **337**, 218–225.
[7] Hou Y, Wang HQ, and Ba Y (2012). High expression of cell division cycle 7 protein correlates with poor prognosis in patients with diffuse large B-cell lymphoma. *Med Oncol* **29**, 3498–3503.
[8] Kim JM, Kakusho N, Yamada M, Kanoh Y, Takemoto N, and Masai H (2008). Cdc7 kinase mediates Claspin phosphorylation in DNA replication checkpoint. *Oncogene* **27**, 3475–3482.
[9] Rainey MD, Harhen B, Wang GN, Murphy PV, and Santocanale C (2013). Cdc7-dependent and -independent phosphorylation of Claspin in the induction of the DNA replication checkpoint. *Cell Cycle* **12**, 1560–1568.
[10] Day TA, Palle K, Barkley LR, Kakusho N, Zou Y, Tateishi S, Verreault A, Masai H, and Vaziri C (2010). Phosphorylated Rad18 directs DNA polymerase eta to sites of stalled replication. *J Cell Biol* **191**, 953–966.
[11] Brandao LN, Ferguson R, Santoro I, Jinks-Robertson S, and Sclafani RA (2014). The role of Dbf4-dependent protein kinase in DNA polymerase zeta-dependent mutagenesis in Saccharomyces cerevisiae. *Genetics* **197**, 1111–1122.
[12] Miller CT, Gabrielse C, Chen YC, and Weinreich M (2009). Cdc7p-Dbf4p regulates mitotic exit by inhibiting Polo kinase. *PLoS Genet* **5**, e1000498.
[13] Murakami H and Keeney S (2014). Temporospatial coordination of meiotic DNA replication and recombination via DDK recruitment to replisomes. *Cell* **158**, 861–873.

[14] Montagnoli A, Tenca P, Sola F, Carpani D, Brotherton D, Albanese C, and Santocanale C (2004). Cdc7 inhibition reveals a p53-dependent replication checkpoint that is defective in cancer cells. *Cancer Res* **64**, 7110–7116.

[15] Montagnoli A, Valsasina B, Croci V, Menichincheri M, Rainoldi S, Marchesi V, Tibolla M, Tenca P, Brotherton D, Albanese C, et al (2008). A Cdc7 kinase inhibitor restricts initiation of DNA replication and has antitumor activity. *Nat Chem Biol* **4**, 357–365.

[16] Tudzarova S, Trotter MW, Wollenschlaeger A, Mulvey C, Godovac-Zimmermann J, Williams GH, and Stoeber K (2010). Molecular architecture of the DNA replication origin activation checkpoint. *EMBO J* **29**, 3381–3394.

[17] Ito S, Ishii A, Kakusho N, Taniyama C, Yamazaki S, Fukatsu R, Sakaue-Sawano A, Miyawaki A, and Masai H (2012). Mechanism of cancer cell death induced by depletion of an essential replication regulator. *PLoS One* **7**, e36372.

[18] Cancer Genome Atlas Research N (2014). Comprehensive molecular profiling of lung adenocarcinoma. *Nature* **511**, 543–550.

[19] Chen YC and Weinreich M (2010). Dbf4 regulates the Cdc5 Polo-like kinase through a distinct non-canonical binding interaction. *J Biol Chem* **285**, 41244–41254.

[20] Oliver TG, Mercer KL, Sayles LC, Burke JR, Mendus D, Lovejoy KS, Cheng MH, Subramanian A, Mu D, Powers S, et al (2010). Chronic cisplatin treatment promotes enhanced damage repair and tumor progression in a mouse model of lung cancer. *Genes Dev* **24**, 837–852.

[21] Kim SH, Ho JN, Jin H, Lee SC, Lee SE, Hong SK, Lee JW, Lee ES, and Byun SS (2016). Upregulated expression of BCL2, MCM7, and CCNE1 indicate cisplatin-resistance in the set of two human bladder cancer cell lines: T24 cisplatin sensitive and T24R2 cisplatin resistant bladder cancer cell lines. *Investig Clin Urol* **57**, 63–72.

[22] Weinreich M and Stillman B (1999). Cdc7p-Dbf4p kinase binds to chromatin during S phase and is regulated by both the APC and the RAD53 checkpoint pathway. *EMBO J* **18**, 5334–5346.

[23] Sheu Y-JJ and Stillman B (2010). The Dbf4-Cdc7 kinase promotes S phase by alleviating an inhibitory activity in Mcm4. *Nature* **463**, 113–117.

[24] Njagi GD and Kilbey BJ (1982). cdc7-1 a temperature sensitive cell-cycle mutant which interferes with induced mutagenesis in Saccharomyces cerevisiae. *Mol Gen Genet* **186**, 478–481.

[25] Ostroff RM and Sclafani RA (1995). Cell cycle regulation of induced mutagenesis in yeast. *Mutat Res* **329**, 143–152.

[26] Sclafani RA, Patterson M, Rosamond J, and Fangman WL (1988). Differential regulation of the yeast CDC7 gene during mitosis and meiosis. *Mol Cell Biol* **8**, 293–300.

[27] Pessoa-Brandao L and Sclafani RA (2004). CDC7/DBF4 functions in the translesion synthesis branch of the RAD6 epistasis group in Saccharomyces cerevisiae. *Genetics* **167**, 1597–1610.

[28] Dyson NJ (2016). RB1: a prototype tumor suppressor and an enigma. *Genes Dev* **30**, 1492–1502.

[29] Chen HZ, Tsai SY, and Leone G (2009). Emerging roles of E2Fs in cancer: an exit from cell cycle control. *Nat Rev Cancer* **9**, 785–797.

[30] Liu H, Tang X, Srivastava A, Pecot T, Daniel P, Hemmelgarn B, Reyes S, Fackler N, Bajwa A, Kladney R, et al (2015). Redeployment of Myc and E2f1-3 drives Rb-deficient cell cycles. *Nat Cell Biol* **17**, 1036–1048.

[31] Kong LJ, Chang JT, Bild AH, and Nevins JR (2007). Compensation and specificity of function within the E2F family. *Oncogene* **26**, 321–327.

[32] Bertoli C, Klier S, McGowan C, Wittenberg C, and de Bruin RA (2013). Chk1 inhibits E2F6 repressor function in response to replication stress to maintain cell-cycle transcription. *Curr Biol* **23**, 1629–1637.

[33] Yamada M, Sato N, Taniyama C, Ohtani K, Arai K, and Masai H (2002). A 63-base pair DNA segment containing an Sp1 site but not a canonical E2F site can confer growth-dependent and E2F-mediated transcriptional stimulation of the human ASK gene encoding the regulatory subunit for human Cdc7-related kinase. *J Biol Chem* **277**, 27668–27681.

[34] Sasi NK, Tiwari K, Soon FF, Bonte D, Wang T, Melcher K, Xu HE, and Weinreich M (2014). The potent Cdc7-Dbf4 (DDK) kinase inhibitor XL413 has limited activity in many cancer cell lines and discovery of potential new DDK inhibitor scaffolds. *PLoS One* **9**, e113300.

[35] Im JS and Lee JK (2008). ATR-dependent activation of p38 MAP kinase is responsible for apoptotic cell death in cells depleted of Cdc7. *J Biol Chem* **283**, 25171–25177.

[36] Chica N, Rozalen AE, Perez-Hidalgo L, Rubio A, Novak B, and Moreno S (2016). Nutritional Control of Cell Size by the Greatwall-Endosulfine-PP2A.B55 Pathway. *Curr Biol* **26**, 319–330.

[37] Mochida S, Ikeo S, Gannon J, and Hunt T (2009). Regulated activity of PP2A-B55 delta is crucial for controlling entry into and exit from mitosis in Xenopus egg extracts. *EMBO J* **28**, 2777–2785.

[38] Ruvolo PP (2016). The broken "Off" switch in cancer signaling: PP2A as a regulator of tumorigenesis, drug resistance, and immune surveillance. *BBA Clin* **6**, 87–99.

[39] Ruiz S, Mayor-Ruiz C, Lafarga V, Murga M, Vega-Sendino M, Ortega S, and Fernandez-Capetillo O (2016). A Genome-wide CRISPR Screen Identifies CDC25A as a Determinant of Sensitivity to ATR Inhibitors. *Mol Cell* **62**, 307–313.

[40] Shimizu H, Nagamori I, Yabuta N, and Nojima H (2009). GAK, a regulator of clathrin-mediated membrane traffic, also controls centrosome integrity and chromosome congression. *J Cell Sci* **122**, 3145–3152.

[41] Naito Y, Shimizu H, Kasama T, Sato J, Tabara H, Okamoto A, Yabuta N, and Nojima H (2012). Cyclin G-associated kinase regulates protein phosphatase 2A by phosphorylation of its B'gamma subunit. *Cell Cycle* **11**, 604–616.

[42] Craney A, Kelly A, Jia L, Fedrigo I, Yu H, and Rape M (2016). Control of APC/C-dependent ubiquitin chain elongation by reversible phosphorylation. *Proc Natl Acad Sci U S A* **113**, 1540–1545.

[43] Foley EA, Maldonado M, and Kapoor TM (2011). Formation of stable attachments between kinetochores and microtubules depends on the B56-PP2A phosphatase. *Nat Cell Biol* **13**, 1265–1271.

[44] Kennedy EK, Dysart M, Lianga N, Williams EC, Pilon S, Dore C, Deneault JS, and Rudner AD (2016). Redundant Regulation of Cdk1 Tyrosine Dephosphorylation in Saccharomyces cerevisiae. *Genetics* **202**, 903–910.

[45] Fuhs SR, Meisenhelder J, Aslanian A, Ma L, Zagorska A, Stankova M, Binnie A, Al-Obeidi F, Mauger J, Lemke G, et al (2015). Monoclonal 1- and 3-Phosphohistidine Antibodies: New Tools to Study Histidine Phosphorylation. *Cell* **162**, 198–210.

[46] Conery AR, Sever S, and Harlow E (2010). Nucleoside diphosphate kinase Nm23-H1 regulates chromosomal stability by activating the GTPase dynamin during cytokinesis. *Proc Natl Acad Sci U S A* **107**, 15461–15466.

[47] Jarrett SG, Novak M, Dabernat S, Daniel JY, Mellon I, Zhang Q, Harris N, Ciesielski MJ, Fenstermaker RA, Kovacic D, et al (2012). Metastasis suppressor NM23-H1 promotes repair of UV-induced DNA damage and suppresses UV-induced melanomagenesis. *Cancer Res* **72**, 133–143.

[48] Stark MS, Woods SL, Gartside MG, Bonazzi VF, Dutton-Regester K, Aoude LG, Chow D, Sereduk C, Niemi NM, Tang N, et al (2012). Frequent somatic mutations in MAP3K5 and MAP3K9 in metastatic melanoma identified by exome sequencing. *Nat Genet* **44**, 165–169.

[49] Meng Z, Moroishi T, and Guan KL (2016). Mechanisms of Hippo pathway regulation. *Genes Dev* **30**, 1–17.

[50] Hergovich A (2013). Regulation and functions of mammalian LATS/NDR kinases: looking beyond canonical Hippo signalling. *Cell Biosci* **3**, 32.

[51] Meng Z, Moroishi T, Mottier-Pavie V, Plouffe SW, Hansen CG, Hong AW, Park HW, Mo JS, Lu W, Lu S, et al (2015). MAP4K family kinases act in parallel to MST1/2 to activate LATS1/2 in the Hippo pathway. *Nat Commun* **6**, 8357.

[52] Tapon N, Harvey KF, Bell DW, Wahrer DC, Schiripo TA, Haber D, and Hariharan IK (2002). salvador Promotes both cell cycle exit and apoptosis in Drosophila and is mutated in human cancer cell lines. *Cell* **110**, 467–478.

[53] Hamilton G and O'Neill E (2013). In: Oren M, Aylon Y, editors. Hippo Pathway and Apoptosis. New York, NY: Springer New York; 2013. p. 117–145.

[54] Matsuoka S, Ballif BA, Smogorzewska A, McDonald ER, Hurov KE, Luo J, Bakalarski CE, Zhao Z, Solimini N, Lerenthal Y, et al (2007). ATM and ATR substrate analysis reveals extensive protein networks responsive to DNA damage. *Science (New York, NY)* **316**, 1160–1166.

[55] Lawrence MS, Stojanov P, Polak P, Kryukov GV, Cibulskis K, Sivachenko A, Carter SL, Stewart C, Mermel CH, Roberts SA, et al (2013). Mutational heterogeneity in cancer and the search for new cancer-associated genes. *Nature* **499**, 214–218.

[56] Campbell JD, Alexandrov A, Kim J, Wala J, Berger AH, Pedamallu CS, Shukla SA, Guo G, Brooks AN, Murray BA, et al (2016). Distinct patterns of somatic genome alterations in lung adenocarcinomas and squamous cell carcinomas. *Nat Genet* **48**, 607–616.

[57] Li CM, Gocheva V, Oudin MJ, Bhutkar A, Wang SY, Date SR, Ng SR, Whittaker CA, Bronson RT, Snyder EL, et al (2015). Foxa2 and Cdx2 cooperate with Nkx2-1 to inhibit lung adenocarcinoma metastasis. *Genes Dev* **29**, 1850–1862.

[58] Dimitrova N, Gocheva V, Bhutkar A, Resnick R, Jong RM, Miller KM, Bendor J, and Jacks T (2016). Stromal Expression of miR-143/145 Promotes Neoangiogenesis in Lung Cancer Development. *Cancer Discov* **6**, 188–201.

[59] Miettinen J, Nordhausen K, and Taskinen S (2017). Blind Source Separation Based on Joint Diagonalization in R: The Packages JADE and BSSasymp. *J Stat Softw* **76**, 31.

[60] Rutledge DN and Jouan-Rimbaud Bouveresse D (2013). Independent Components Analysis with the JADE algorithm. *TrAC Trends Anal Chem* **50**, 22–32.

[61] Anne Biton AZ, Barillot Emmanuel, and Radvanyi François (2016). MineICA: Independent component analysis of transcriptomic data.

[62] Subramanian A, Tamayo P, Mootha VK, Mukherjee S, Ebert BL, Gillette MA, Paulovich A, Pomeroy SL, Golub TR, Lander ES, et al (2005). Gene set enrichment analysis: a knowledge-based approach for interpreting genome-wide expression profiles. *Proc Natl Acad Sci U S A* **102**, 15545–15550.

[63] Liberzon A, Birger C, Thorvaldsdottir H, Ghandi M, Mesirov JP, and Tamayo P (2015). The Molecular Signatures Database (MSigDB) hallmark gene set collection. *Cell Syst* **1**, 417–425.

[64] Lerdrup M, Johansen JV, Agrawal-Singh S, and Hansen K (2016). An interactive environment for agile analysis and visualization of ChIP-sequencing data. *Nat Struct Mol Biol* **23**, 349–357.

[65] Robinson JT, Thorvaldsdottir H, Winckler W, Guttman M, Lander ES, Getz G, and Mesirov JP (2011). Integrative genomics viewer. *Nat Biotechnol* **29**, 24–26.

[66] Zhang JH, Chung TD, and Oldenburg KR (1999). A Simple Statistical Parameter for Use in Evaluation and Validation of High Throughput Screening Assays. *J Biomol Screen* **4**, 67–73.

[67] Birmingham A, Selfors LM, Forster T, Wrobel D, Kennedy CJ, Shanks E, Santoyo-Lopez J, Dunican DJ, Long A, Kelleher D, et al (2009). Statistical methods for analysis of high-throughput RNA interference screens. *Nat Methods* **6**, 569–575.

[68] Britto R, Sallou O, Collin O, Michaux G, Primig M, and Chalmel F (2012). GPSy: a cross-species gene prioritization system for conserved biological processes–application in male gamete development. *Nucleic Acids Res* **40**, W458–W465.

[69] Tranchevent LC, Barriot R, Yu S, Van Vooren S, Van Loo P, Coessens B, De Moor B, Aerts S, and Moreau Y (2008). ENDEAVOUR update: a web resource for gene prioritization in multiple species. *Nucleic Acids Res* **36**, W377–W384.

[70] Chen J, Bardes EE, Aronow BJ, and Jegga AG (2009). ToppGene Suite for gene list enrichment analysis and candidate gene prioritization. *Nucleic Acids Res* **37**, W305–W311.